RSC Advances

ROYAL SOCIETY OF CHEMISTRY

www.rsc.org/advances

RSC Advances RSCPublishing

ARTICLE

Tuning the size and upconversion emission of $NaYF_4$: Yb^{3+}/Pr^{3+} nanoparticles through Yb^{3+} doping

Cite this: DOI: xoxxoooooox

Shuwei Hao,[a] Wei Shao ,[a] Hailong Qiu,[a] Yunfei Shang ,[a] Rongwei Fan ,[c] Xuyun Guo,[d] Lili Zhao,[a,e] Guanying Chen*,[a,b] and Chunhui Yang*[a]

We introduce a simple method to tune the resulting size as well as the upconversion luminescence of $NaYF_4$:Yb^{3+}/Pr^{3+} nanoparticles through varying the sensitizer ytterbium concentration. Varied amount of ytterbium from 10-70% were doped into the fluoride nanoparticles, producing a tunable resulting size from 29 to 153 nm. Meanwhile, the blue upconversion luminescence intensity of $NaYF_4$:Yb^{3+}/Pr^{3+} nanoparticle was monotonously enhanced, reaching a maximum ~3.4 fold enhancement at ytterbium concentration of 70% owing to an improved energy transfer from the ytterbium to the praseodymium ions. Moreover, the luminescence intensity ratio of the blue to the green upconversion was tailored by the composition-dependent cross relaxation process. The result here provides a paradigm for simultaneous control of the physical dimension as well as the luminescence properties of lanthanide-doped upconversion nanoparticles.

Introduction

Lanthanide-doped upconversion nanoparticles (UCNPs) have attracted a great deal of consideration due to their intriguing optical properties that promise their potential applications in fields as diverse as solid-state lasers[1], optical data storage[2], solar energy conversion[3-6], biological imaging[7-10], and photodynamic therapy [11,12]. UCNPs are able to convert two or more long wavelength light photons into short wavelength emissions through the use of energy level of trivalent lanthanide ion that is embedded into an inorganic host lattice. In particular, lanthanide doped fluoride UCNPs generally exhibit the highest upconversion (UC) or downconversion (DC) efficiency [3], as the fluoride materials have high physicochemical stabilities, as well as intrinsic low phonon energies (<350 cm^{-1}) that are able to minimize energy losses at the intermediate states of lanthanide ions. Typically, UCNPs of $NaYF_4$ doped with a sensitizer Yb^{3+} and an activator of Er^{3+}, Ho^{3+} or Tm^{3+} has been of extensive study, and considered to be one of the most efficient UC systems [13]. This is not only because the sensitizer Yb^{3+} has a unique one excited energy $^2F_{5/2}$ (~10000 cm^{-1}) which possesses a significantly higher extinction coefficient (typically ~10l $mol^{-1}cm^{-1}$) and which matches the ladder-like energy gaps of the Er^{3+}, Ho^{3+} or Tm^{3+} ions to empower efficient resonant energy transfers to produce efficient UC emissions[14-18]. However, limited success has been met in $NaYF_4$-based UCNPs doped with other lanthanide ions like Pr^{3+} ion that has a unique pattern of energy levels.

The Pr^{3+} ion has been of great use as multi-wavelength laser activator or colored emitting ions, as it offers the possibility to achieve a simultaneous blue, green or red emission lasing or other purposes [19]. Visible UC lasers at multiple wavelengths have been realized in Pr^{3+} doped ZBLAN (Zr-Ba-La-Al-Na) bulk glass under an infrared laser pump at ~ 840 nm [20]. Laser action of the blue UC from the transition of the excited $^3P_0$ state to the ground $^3H_4$ state has been demonstrated in various bulk crystals, involving the frequency conversion mechanisms of either excited state absorption or photon

avalanche [1,21-23]. Moreover, yellow-to-blue frequency UC processes in Pr^{3+} ions have also been extensively studied in a range of low phonon crystals and glass [24,25], while intense white light emitting were developed in Pr^{3+}/Er^{3+} co-doped tellurite glass sensitized by Yb^{3+} ion [27]. Despite successes on Pr^{3+}-doped bulk materials, till this point, limited investigation has been devoted to Pr^{3+}-doped nanoparticles. The relative work in literature is on visible UC in Yb^{3+}/Pr^{3+} co-doped Y_2O_3 nanoparticles [26]. However, the employed low Yb^{3+} concentration of 1-2 mol% produces a low UC efficiency owing to the large Yb^{3+}- Pr^{3+} ion-ion distance that limits the efficiency of energy transfer from the Yb^{3+} to the Pr^{3+}. It is noted that the sensitizer Yb^{3+} ion has an exclusive excited state; increase of its concentration, therefore, exclude the possibility producing cross relaxation process induced quenching effect. Varying Yb^{3+} concentration to shorten the sensitizer-activator distance is an important approach to enhance UC luminescence; this conclusion has been verified by Duan *et al*, Han *et al.* as well as by our group in Yb^{3+}/Tm^{3+}-codoped $NaYF_4$ and YF_3 UCNPs [28-34]. On the other hand, doping of trivalent lanthanide ions into nanomaterials can influence its growth dynamics due to the dopant-induced transient electric dipole on the surface of the growing nanoparticles [35-37]. For example, our group showed that varying dopant concentration of Yb^{3+} or Gd^{3+} can tune the size and phase of the resulting multifunctional CeO_2 oxide nanoparticles [37]. Here, we show that varying the sensitizer Yb^{3+} concentration in Yb^{3+}/Pr^{3+}-codoped $NaYF_4$ nanoparticles not only can produce a size-tunable UNCPs, but also can produce enhanced and tailor upconversion emissions from the Pr^{3+} ion under ~980 nm NIR light exciation.

Results and discussion

The ionic radii of Yb^{3+} (0.868Å) and Y^{3+} (0.893Å) are different, which may result in the variation of size and morphology in the formation of $NaREF_4$ UCNPs. We prepared $NaYF_4$: Yb^{3+}/Pr^{3+} UCNPs doped with varied Yb^{3+} ion concentrations of 10-70 mol%. During the synthesis, all synthetic parameters were kept exactly the same, except for varying the doping concentration of Yb^{3+} ions. Fig. 1 (a)-(d) displays the transmission electron microscopy (TEM) images of $NaYF_4$ UCNPs doped with 10, 30, 50, 70 mol% Yb^{3+}, respectively. High resolution TEM imaging and selected area electron diffraction patterns confirmed the high crystallinity and hexagonal phase of all resulting nanoparticles (Fig. S1, supporting information). The energy dispersive x-ray spectra (EDAX) indicate that the elemental content of the resulting $NaYF_4$: Yb^{3+}/Pr^{3+} UCNPs is in general agreement with the mixture of cationic precursor, suggesting stoichiometric doping of Yb^{3+} ions at a precisely defined concentration (Fig. S2, supporting information). The results demonstrate that all the rare earth ions can be effectively incorporated into the final UCNPs with our synthetic conditions. Therefore, the Yb^{3+} and Pr^{3+} doping concentration can be readily controlled by varying the initial reactant ratio.

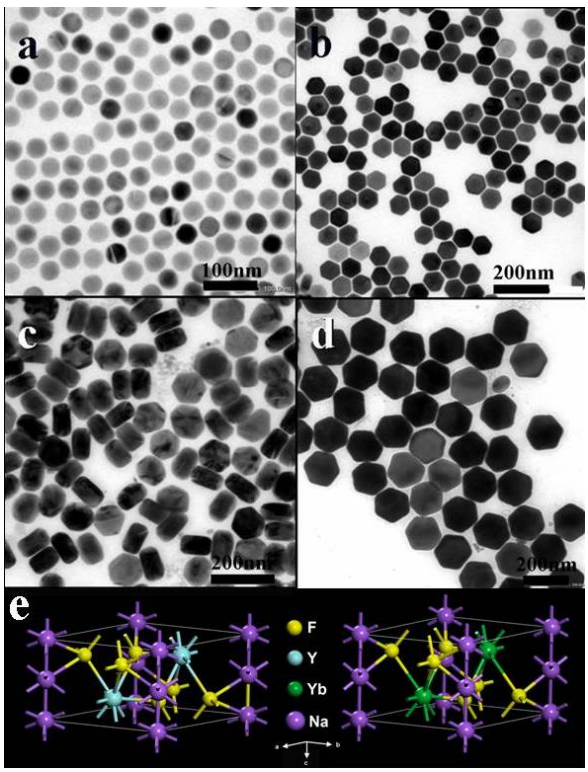

Fig. 1 Transmission electron images for $NaYF_4$ nanocrystals codoped with 0.5% Pr^{3+} and various concentration of (a) 10% Yb^{3+}, (b) 30% Yb^{3+}, (c) 50% Yb^{3+}, and (d) 70% Yb^{3+}. (e) Schematic representation of the hexagonal structure of $NaYF_4$ or $NaYbF_4$ nanoparticles (a=b=6.245Å, c=4.392Å for $NaYF_4$ and a=b=5.912Å, c=4.653Å for $NaYbF_4$).

As one can see in Fig. 1 (a), very small ~29 nm sphere-like UCNPs were formed for Yb^{3+} concentration of 10%. However, it evolves into larger ~ 62 nm hexagonal-shape UCNPs when Yb^{3+} concentration of 30% were doped [Fig. 1 (b)]. For higher Yb^{3+} concentration of 50 and 70%, the hexagonal shape remains unchanged, yet the size increased further to 103 and 153 nm, respectively [Fig. 1(c) and (d)]. These results agree with the corresponding histogram of the average size distribution (Supporting

information, Fig. S3). The size evolution can be attributed to the Yb^{3+}-varied crystal growth rate via the modification of electron charge density on the nanoparticle surface. Liu *et al.* calculated, based on density functional theory (DFT), that the electron charge density of the crystal surface was increased when a Y^{3+} (0.893Å) ion in $NaYF_4$ was replaced by a larger Gd^{3+} (0. 938Å) ion, which thus repelled the anion F^- to produce a smaller nanoparticle size [35]. Therefore, when Y^{3+} (0.893Å) is replaced by a smaller Yb^{3+} (0.868Å) ion replacing, the electron charge density on the surface of growing UCNPs will be decreased, thus allowing more attraction of F^- ion to the particle surface to form a larger size UCNPs.

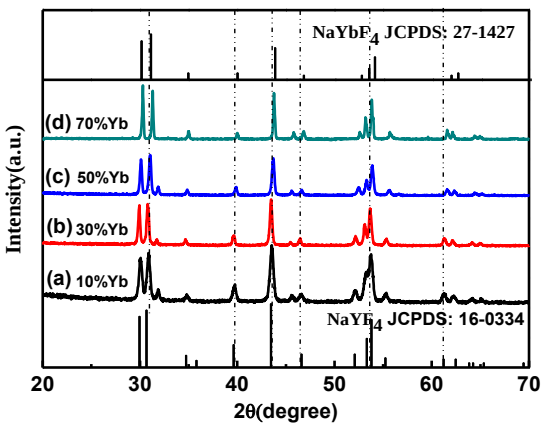

Fig. 2 The XRD pattern of $NaYF_4$ nanoparticles codoped with 0.5% Pr^{3+} and various concentration of Yb^{3+} ions of (a) 10% Yb^{3+}, (b) 30% Yb^{3+}, (c) 50% Yb^{3+}, and (d) 70% Yb^{3+}. The standard XRD patterns of hexagonal phase $NaYF_4$ and $NaYbF_4$ are also plotted as a reference.

The crystalline phases of as-prepared samples were further determined by powder X-ray diffraction (XRD); the result is shown in Fig. 2. The XRD pattern for the sample doped with Yb^{3+} of 10 mol% is in good agreement with the standard hexagonal phase $NaYF_4$ (JCPDS 16-0334), confirming the formation of a hexagonal crystal phase. A sequential shifting of the XRD peaks is observed towards high-angle when higher Yb^{3+} concentration were doped. This peak shifting indicates the decrease of a unit-cell volume due to the replacement of Y^{3+} by smaller ion radii Yb^{3+}. In other words, the hexagonal phase $NaYF_4$ gradually transforms to hexagonal phase $NaYbF_4$ when elevated Yb^{3+} concentration was doped.

It is interesting to note that doping of varied Yb^{3+} concentration also produced important influence on the UC luminescence. Fig. 3 shows the emission spectra of $NaYF_4$ UCNPs codoped with 0.5% Pr^{3+} and varied Yb^{3+} ion concentrations of (a) 10%, (b) 30%, (c) 50%, (d) 70%, respectively, under ~ 980nm laser excitation. All UCNPs exhibit the typical blue emission band at ~486 nm, the green emission band at ~523 nm, the green emission band at ~540 nm, the red emission band at ~605 nm, as well as the red emission band at ~639 nm, being ascribed to the $^3P_0 \rightarrow {}^3H_4$, $^1I_6 \rightarrow {}^3H_5$, $^3P_1 \rightarrow {}^3H_5$, $^3P_0 \rightarrow {}^3H_6$ and $^3P_0 \rightarrow {}^3F_2$ transitions of Pr^{3+} ions, respectively. As one can see in Fig. 3, the blue emission at 486 nm is increased gradually when elevating the Yb^{3+} concentration, and enhances about ~ 3.4 times for Yb^{3+} of 70%. We also compared the luminescence intensity of $NaYF_4$:70%Yb^{3+}/0.5%Pr^{3+} with that of well-investigated hexagonal $NaYF_4$:20%Yb^{3+}/0.5%Er^{3+} and $NaYF_4$: 20%Yb^{3+}/0.5%Tm^{3+} nanocrystals (size ~30 nm) (Supporting information, Fig. S4); it is lower than that of the typical $NaYF_4$:20%Yb^{3+}/0.5%Er^{3+} and $NaYF_4$: 20%Yb^{3+}/0.5%Tm^{3+} systems. This result indicates that a further design of this Yb^{3+}/Pr^{3+} codoped system is in need to increase its upconversion efficiency to compete with currently well-known Yb^{3+}/Ho^{3+} and Yb^{3+}/Tm^{3+} UC systems.

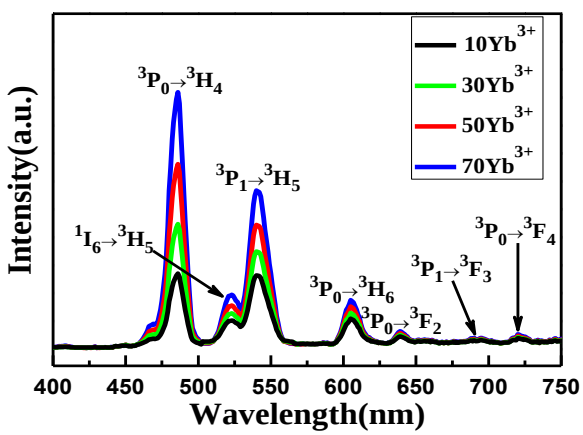

Fig. 3 UC emission spectra of colloidal $NaYF_4$ nanocrystals codoped with 0.5% Pr^{3+} and various concentrations of Yb^{3+} ions (10-70%) under diode laser excitation at 980 nm.

To shed light on the enhancement mechanism of blue UC emission as well as the population process of upper excited $^3P_0$ levels of Pr^{3+} ions, the dependence of the intensities of various UC emission peaks on laser power for $NaYF_4$:10%Yb^{3+}/0.5%Pr^{3+} UCNPs were measured and displayed in Fig. 4. For an unsaturated UC process, the number of photons that are involved to populate the upper emitting state can be obtained by the relation

$$I_{UC} \propto P^n, \quad (1)$$

where I_{UC} is the UC intensity, P is the pump laser power, and n is the number of laser photons involved to populate the upper emitting levels. The value of n can be determined by the slope value of a linear fitting in a logarithmic-logarithmic plot of equation (1). As shown in Fig. 4, slope values of 1.98, 1.91, 1.89, and 1.75 were observed for UC emissions peaked at 486, 523, 540, and 639 nm, respectively, for $NaYF_4$: 10%Yb^{3+}/0.5% Pr^{3+} UCNPs. These slope values agree well with the previous results that in Yb^{3+}-Pr^{3+} codoped bulk materials under continuous wave laser excitation at ~980 nm [38]. This result illustrates that two-photon processes are involved to populate the $^1I_6$, $^3P_1$ and $^3P_0$ states, respectively (consult Fig. 5). It is noted that the blue emission at 486 nm and the green emissions at 540nm have the same slope value of ~2 (see Fig. 5). The mechanisms for blue, green, and red UC generation are presented in Fig. 5.

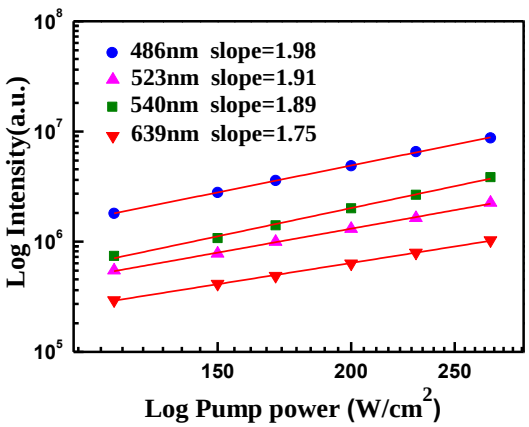

Fig. 4 Log–log plots of the intensities of various UC emission bands in Fig. 3 on the excitation density in $NaYF_4$ nanoparticles codoped with 10 mol% Yb^{3+} and 0.5 mol% Pr^{3+}. The slope values of the linear fits (solid line) are presented in the inset together with the peak wavelength of each UC band.

Fig. 5 depicts the pertinent energy levels of the Pr^{3+} and Yb^{3+} ions as well as the proposed UC mechanisms [27]. Laser photons at ~ 980 nm match the $^2F_{7/2}\rightarrow{}^2F_{5/2}$ transition of Yb^{3+} ion, resonantly exciting Yb^{3+} ion from the ground to its excited state. Energy transfer process from the Yb^{3+} ions to a neighboring Pr^{3+} ion can promote the Pr^{3+} ions in the $^3H_4$ state to $^1G_4$ state (ET1). The population in the $^1G_4$ level can be promoted to the $^3P_0$ levels either by energy transfer (ET2) from another excited Yb^{3+} ion or absorbing the energy of pumping photon. Once the $^3P_0$ level is populated, the excited electron can release its energy by emitting visible emissions. The blue emission at 486 nm can be produced by radiative decay to the ground state from the $^3P_0$ state. Generally, the pumping energy of 980 nm is very difficult to population in $^3P_1$ and higher states of Pr^{3+} ions. But the cross relaxation between $^3P_0\rightarrow{}^3P_2$ and $^3H_5\rightarrow{}^3H_4$ in Pr^{3+} ions promotes the occupation in the $^3P_2$ state, which through nonradiative relaxation process populate $^1I_6$ and $^3P_1$ states. Excited Pr^{3+} ions in $^1I_6$ and $^3P_1$ states decay to $^3H_5$ state, leading to green emission centered at 523 and 540 nm. The red emissions at 605 and 639 nm originate from the $^3P_0$ state to $^3H_6$ and $^3F_2$ transitions, respectively.

It is noted that the efficiency of cross relaxation processes strongly depends on the Pr^{3+} ion's distribution, while the efficiency of ET1 and ET2 processes are insensitive to Pr^{3+} ion concentration in the host lattice when varying in a small amount range.

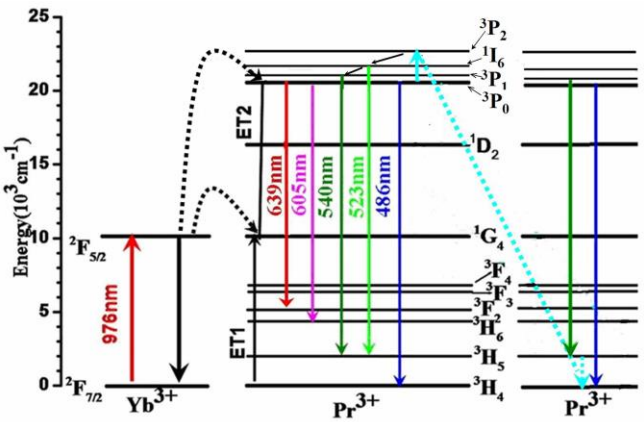

Fig. 5 Energy level diagram of the Pr^{3+} and Yb^{3+} ions as well as the proposed UC mechanism in $NaYF_4$: Yb^{3+}/Pr^{3+} nanocrystals via varying content of Yb^{3+} ions under a 980 nm laser excitation.

As a result, we further prepared $NaYF_4$ nanoparticles codoped with Yb^{3+} of 10%, and various Pr^{3+} concentrations of 0.1%, 0.25%, 0.5%, and 1% Pr^{3+}. The UC spectra from them are displayed in Fig. 6(a). The intensity increases slightly when the Pr^{3+} concentration is increased from 0.1 to 0.5% molar fraction. This augment of emission intensity can be ascribed to the increased number of emitting Pr^{3+} centers. However, a further increase in the Pr^{3+} concentration results in a decrease in the emission intensity. This is partly because, for a given doping content of Yb^{3+} and overall excitation energy, the excitation received by individual Pr^{3+} ion decreased with the increase of Pr^{3+} ion concentration. More importantly, the high concentration of Pr^{3+} ions leads to a decrease in distance between Pr^{3+} ions, which enhances the probability of cross-relaxation, and thus suppresses the efficient energy transfer processes from Yb^{3+} ions to Pr^{3+} ions for

population of $^3P_0$ state, resulting in an increase in green/blue ratio with the increase of Pr^{3+} concentration [Fig. 6(b)]. It is noted that the intensity ratio of the band 540 nm to the band at 639 nm remain almost unchanged. This is because they arise from the same upper excited energy level of the $^3P_0$ state.

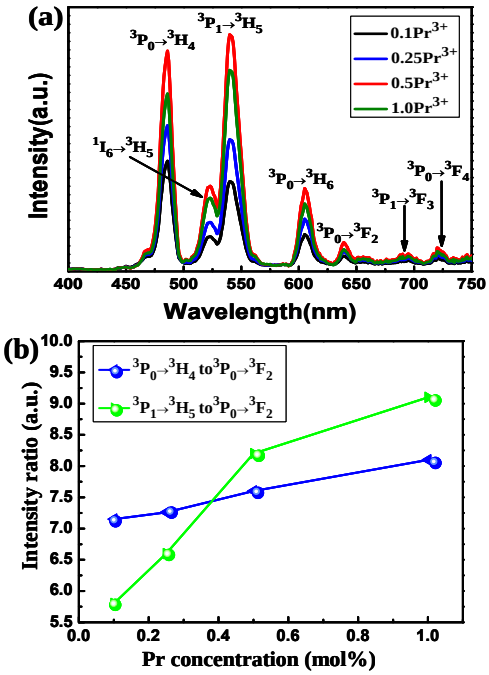

Fig. 6 (a) UC emission spectra of $NaYF_4$: Yb^{3+}/Pr^{3+} nanoparticles codoped with Yb^{3+} of 10%, and various concentrations of Pr^{3+} ions (0.1-1%) under diode laser excitation at 980 nm. (b) The intensity ratios of emissions at 486 nm (from the $^3P_1$ state to the $^3H_4$ state), at 540 nm (from the $^3P_0$ state to the $^3H_5$ state), to the emission at 639 nm (from the $^3P_0$ state to the $^3F_2$ state) versus Pr^{3+} concentration.

Fig. 7 shows the variation of UC emissions from $NaYF_4$: $10\%Yb^{3+}/0.5\%Pr^{3+}$ UCNPs when irradiated with a varied pump power. For low pump power the intensity for emission at 486 nm is lower than that of the emission at 540 nm, while a reverse result is obtained under high pump power. This switching result illustrates that high laser irradiance also facilitates the increase of blue UC emission in $NaYF_4$: $10\%Yb^{3+}/0.5\%Pr^{3+}$ nanoparticles. It is reasonable to assume that, for the given Yb^{3+} concentration in the samples, the excitation received by individual Pr^{3+} ions increased with the enhancement of laser irradiance.

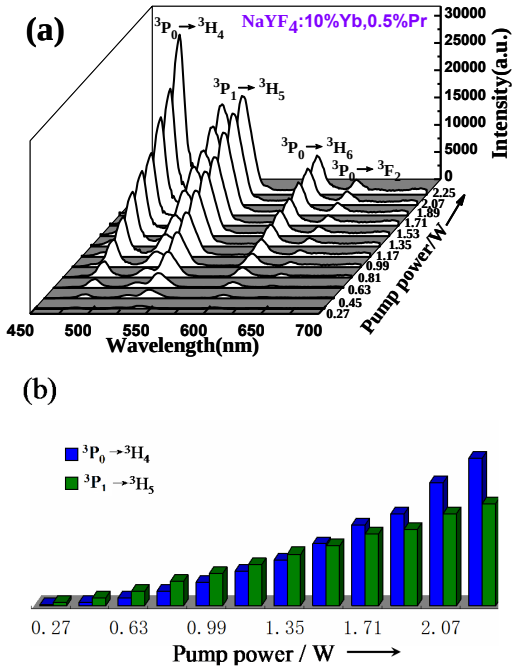

Fig. 7 (a) Pump-power-dependent UC 4f emission spectra of $NaYF_4$: $10\%Yb^{3+}/0.5\%Pr^{3+}$ UCNPs. All spectra were recorded at room temperature under excitation of ~ 980 nm diode laser at a power density of 5 Wcm^{-2}. (b) Emission intensities for the $^3P_1 \rightarrow {}^3H_4$ transition and the $^3P_0 \rightarrow {}^3H_5$ transition from $NaYF_4$: $10\%Yb^{3+}/0.5\%Pr^{3+}$ UCNPs as a function of laser pump power.

Conclusions

In summary, we have demonstrated that varying the sensitizer Yb^{3+} concentration can simultaneously tune the resulting size as well as the upconversion luminescence of $NaYF_4$:Yb^{3+}/Pr^{3+} UNCPs. The intensity of the blue UC emission was enhanced by ~3.4 fold when elevating the sensitizer concentration from 10 to 70%, being ascribed to the improved energy transfer from the Yb^{3+} to Pr^{3+} ions due to the shorter distance between them. The intensity ratio of the blue to the green upconversion was also varied by the composition-dependent cross relaxation process. The reported result might have important implications in other lanthanide-doped UCNPs that involve the use of Yb^{3+} as sensitizer ions.

Acknowledgements

This work is supported by Natural Science Foundation of China (51102066 and 51402071), the Fundamental Research Funds for the Central Universities (Grant No. HIT. NSRIF.2015048), international scientific and technological cooperation projects (Grant No. 2014DFA50740) and the National Science Fund for Distinguished Young Scholars (Grant No. 51325201).

Notes and references

[a] School of Chemical Engineering and Technology, Harbin Institute of Technology, 150001 Harbin, People's Republic of China.
[b]Institute for Lasers, Photonics and Biophotonics, Department of Chemistry, University at Buffalo, The State University of New York, Buffalo, NY 14260, USA.
[c]National Key Laboratory of Tunable Lasers, Institute of Optical-Electronics, Harbin Institute of Technology, 150001 Harbin, People's Republic of China
[d]Department of Chemistry, the Hong Kong University of Scienece and Technology, Clear water Bay, Hong Kong SPA.
[e]Harbin Huigong Technology Co., Ltd.
E-mails: guanying@buffalo.edu
yangchh@hit.edu.cn

1 F. Auzel. Chem. Rev., 2004, **104**, 139.
2 E. Downing, L. Hesselink, J. Ralston, R. Macfarlane. Science, 1996, **273**, 1185.
3 W. Q. Zou1, C. Visser, J. A.Maduro1, M. S. Pshenichnikov, J. C. Hummelen. Nature Photonics, 2012, **6**, 561**.**
4 C. Z. Yuan, G. Y. Chen, P. N. Prasad, T. Y. Ohulchanskyy, Z. J. Ning, Haining Tian, L. C. Sund and H. Agren. J. Mater. Chem., 2012, **22**, 16709.
5 G. Y. Chen, J. W. Seo, C. H. Yang and P. N. Prasad. Chem. Soc. Rev., 2013, **42**, 8304.
6 Y. N. Qian, R. Wang, B. Wang, B. F. Zhanga and S. P. Gao. RSC Adv., 2014, **4**, 6652.
7 J. Zhou, Z. Liu, and F. Li. Chem. Soc. Rev., 2012, **41**, 1323.
8 T. S. Yang, Q. L., J. C Li, S. Z. Pu, P. Y. Yang and F. Y. Li. RSC Adv., 2014, **4**, 15613.
9 G. Y. Chen, C. H. Yang, and P. N. Prasad. Acc. Chem. Res., 2013, **46**, 1474.
10 S. W. Hao, G. Y. Chen and C. H. Yang. Theranostics. 2013, **3**, 331.
11 N. Muhammad Idris, M. K. Gnanasammandhan, J. Zhang, P. Ho, R. Mahendran, and Y. Zhang. Nature Med., 2013, **18**, 1580.
12 G. Y. Chen, H. L. Qiu, P. N. Prasad and X. Y. Chen. Chem. Rev., 2014, **114**, 5161.
13 F. Wang , X. G. Liu. Chem. Soc. Rev., 2009, **38** , 976.
14 M. Haase and H. Schäfer, Angew. Chem. Int. Ed., 2012, **50**, 5808.
15 S. Heer, K. Kompe, H. U. Gudel, M. Haase. Adv. Mater., 2004, **16**, 2102.
16 C. Li, J. Yang, Z. Quan, P. Yang, D. Kong, J. Lin. Chem. Mater., 2007, **19**, 4933.
17 D. Q. Chen and P. Huang. Dalton Trans., 2014, **43**, 11299.
18 D. Q. Chen, Y. Chen, H. W. Lu and Z. G. Ji. Inorg. Chem., 2014, **53**, 8638.
19 R. Piramidowicz, R. Mahiou, P. Boutinaud, M. Malinowski. Appl. Phys. B, 2011, 104, 873.
20 H. M. Pask and A. C. Hanna. Opt. Commun., 1997, 134, 139.
21 L. D. Merkle, B. Zandi, Y. Guyot, H.R. Verdun, B. McIntosh, B. H. T. Chai, J. B. Gruber, M. D. Seltzer, C. A. Morrison, R. Moncorge. Advanced Solid-State Lasers, 1994, 20, 361.
22 L. Esterowitz, R. Allen, M. Krueger, F. Bartoli, L. S. Goldber, H. P. Jenssen, A. Linz, V.O. Nicolai. J. Appl. Phys., 1977, 48, 650.
23 T. Danger, T. Sandrock, E. Heumann, G. Huber, B. Chai. Appl. Phys. B, 1993, 57, 239.
24 R. Balda, J. Fernandez, A. Mendioroz,M. Voda, M. Al-Saleh. Opt. Mater., 2003, 24, 91.
25 A. Remillieux, B. Jacquier, C. Linares, C. Lesergent, S. Artigaud, D. Bayard, L. Hamon, J.L. Beylat, J. Phys. D. Appl. Phys., 1996, 29, 963.
26 C. B. Zheng, Y. Q. Xia, F. Qin, Y. Yu, J. P. Miao, Z. G. Zhang , W. W. Cao, Chem. Phys. Let., 2010, 496, 316.
27 Y. Dwivedi, R. Anita, and S. B. Rai. Journal of Applied Physics, 2008, 104, 043509.
28 H. L. Qiu, G. Y. Chen, R. W. Fan, L. M. Yang, S. W. Hao, C. H. Yang and P. N. Prasad. Nanoscale, 2014, 6, 753-757.
29 G. Y. Chen, T. Y. Ohulchanskyy, R. Kumar, H. Ågren, and Paras N. Prasad. ACS Nano, 2011, 4, 3163.
30 H. Zhang, Y. J. Li, Y. C. Lin, Y. Huang and X. F. Duan. Nanoscale, 2011, 3, 963.
31 G. Y. Chen, T. Y. Ohulchanskyy, W. C. Law, H. Ågren, and P. N. Prasad. Nanoscale, 2011, 3, 2003.
32 G. Y. Chen , J. Shen, T. Y. Ohulchanskyy, N. J. Patel, A. Kutikov, Z. P. Li, J. Song, R. K. Pandey, H. Ågren, P. N. Prasad and G. Han. ACS Nano, 2012, 6, 8280.
33 J. Shen, G. Y. Chen, T. Y. Ohulchanskyy, S. J. Kesseli, S. Buchholz, Z. P. Li, P. N. Prasad and G. Han. Small, 2013, 9, 3213.
34 A. Punjabi, X. Wu, A. T. Apollon, M. E. Rifai, H. Lee,Y. W. Zhang, C. Wang, Z. Liu, E. M. Chan, C. Y Duan and G. Han. ACS Nano, 2014, DOI: 10.1021/nn505051d
35 F. Wang, Y. Han, C. S. Lim, Y. H. Lu, J. Wang, J. Xu, H. G. Chen, C. Zhang, M. H. Hong, X. G. Liu. Nature, 2010, 463, 1061.
36 D. Chen and Y. Wang. Nanoscale, 2013, 5, 4621-4637.
37 H. Qiu, G. Chen, R. Fan, C. Cheng, S. Hao, D. Chen, and C. Yang. Chem. Commun., 2011, 47, 9648-9650.
38 R. Balda, J. Fernandez, A. Mendioroz, M. Voda, and M. Al-Saleh. Phys. Rev. B, 2003, 68, 165101.